IEEE Open Journal of Antennas and Propagation

Received XX Month, XXXX; revised XX Month, XXXX; accepted XX Month, XXXX; Date of publication XX Month, XXXX; date of current version XX Month, XXXX.

Digital Object Identifier 10.1109/OJAP.2020.1234567

Predicting the Maximum Achievable Antenna Bandwidth and Efficiency Using Machine Learning: a Terminal-Integrated Meander IFA Case Study

Julian Roqui, *Student Member, IEEE*, Alain Pegatoquet, *Member, IEEE*, Luca Santamaria, *Student Member, IEEE*, Leonardo Lizzi, *Senior Member, IEEE*

[1]Université Côte d'Azur, CNRS, LEAT, Sophia Antipolis, 06903, France

CORRESPONDING AUTHOR: leonardo.lizzi@univ-cotedazur.fr.

ABSTRACT In this paper, an approach based on Machine Learning (ML) to predict the maximum achievable performance (fractional bandwidth and total efficiency) of a printed Inverted F-antennas (IFAs) integrated into compact IoT terminals is proposed. This original approach relies on the use of a Multi-Layer Perceptron (MLP) artificial neural network (ANN), which is trained using data from numerical simulations that take into account the constraints of practical implementations. The effectiveness of the approach is demonstrated through comparisons with numerical and experimental results, as well as with theoretical results available in the literature. The obtained results show that the proposed supervised regression ML model is capable of predicting the maximum achievable fractional bandwidth and total efficiency, with an accuracy of 95.9% and 98.6%, respectively.

INDEX TERMS Integrated antennas, terminal antennas, machine learning, inverted-F antennas (IFA), artificial neural networks, internet-of-things (IoT).

I. INTRODUCTION

BY the end of 2023, the number of connected devices had reached 16.6 billion. This figure is projected to increase by 18%, reaching 18.8 billion by the end of 2024 [1]. A significant driver of this growth is the rise in machine-to-machine (M2M) communication devices, which support applications such as smart meters, video surveillance, health-care monitoring, transportation, and asset or package tracking [2].

The wireless connectivity of these M2M devices relies very often on the use of compact antennas, embedded as a part of the terminal's Printed Circuit Board (PCB) or chassis. Their design is a challenging task for two main reasons: their miniaturization (the dimensions of these antennas must usually be much smaller than the wavelength at the working frequency), and the constraints imposed by the applications (e.g., position of the antenna clearance area, use of low-cost materials, etc.) These constraints limit the achievable antenna performance. Therefore, having an a-priori (prior to the antenna design) estimation of the maximum performance that antennas embedded in M2M devices can achieve would be particularly useful. On one hand, it would allow the antenna designer to have an idea of which antenna characteristics should be targeted given the application constraints, and how they will reflect on the overall system performance. On the other hand, it would provide the antenna designer with a benchmark for assessing the quality of specific antenna solutions.

From a theoretical point of view, the prediction of the antenna performance bounds is a problem that has been widely investigated in the last decades [3].

Initial works focused on antenna bandwidth. In 1947, Wheeler derived a bandwidth limit for some selected antenna structures using circuit models [4]. A year later, Chu used a technique based on equivalent circuits to set a lower bound on the antenna quality factor (Q-factor), which is strictly related to the bandwidth, starting from the spherical modes outside the sphere circumscribing the antenna [5]. Despite Chu's bound being considered as a reference, it turned out to be too optimistic as it does not take into account the

energy between the surface of non-spherical antennas and the enclosing sphere.

Several enhancements have been therefore proposed over the years. In [6], the Q bound was calculated by analytically integrating the electromagnetic field generated by the antenna, but still considering spherical (or cylindrical) modes. In [7], McLean proposed an exact expression for the minimum Q that refined Chu's result in the upper end of the range of antenna size which is considered electrically small. In [8], Thal established a tighter bound on Q for any antenna consisting of conductors on the surface of an empty or material-filled sphere.

More recently, the works by Gustafsson et al. [9], Yahgjian and Stuart [10], Chalas [11], and Thal [12] overcame the limitation of considering the current distributed within a spherical region, opening the way to the definition of Q bounds for antennas of arbitrary shape. This was obtained using different approaches that consider stored energies.

If the bounds on Q and bandwidth have been widely investigated, research on antenna efficiency is more limited. As usual, works initially focused on specific geometries (e.g., planar structures [13]) to later extend to any antenna shape. In [14] and [15], the efficiency maximization problem has been reformulated as an optimization problem for finding the optimal current distribution. Differently, the prediction of the efficiency bound is obtained by assuming constant current in [16] or by using the circuit theory in [17], [18].

Despite these works (and many more that could be cited) providing a better understanding of the limitations imposed by the physics on the antenna performance, their usefulness for an antenna engineer designing a PCB-printed antenna embedded into a compact M2M device is limited. As a matter of fact, when an engineer designs an antenna, the gap between its performance and the theoretical bounds depends on two factors: (a) the antenna designer's ability, and (b) the difference between the assumptions made to determine the theoretical bound and the design practical constraints. Because of this latter point, the theoretical bound can neither be used as a benchmark for evaluating the quality of an antenna design, nor as an prediction of the antenna performance to be targeted during the design process.

In this paper, a novel approach to predict the maximum achievable antenna bandwidth and total efficiency of printed Inverted F-antennas (IFAs) integrated into compact IoT terminals is proposed. The decision to focus solely on fractional bandwidth and total efficiency is based on two main reasons. First, these two criteria are the most relevant when considering terminal-integrated IFA antennas. Radiation pattern characteristics are less critical, as this specific antenna configuration typically exhibits omnidirectional radiation due to the presence of the PCB ground plane, which contributes to the antenna radiation. Consequently, including radiation characteristics such as directivity is not worthwhile, since these parameters remain relatively constant given the antenna-terminal configurations studied. Second, incorporating additional performance metrics would require more output neurons, complicating the neural network's architecture. This would lead to reduced generalization ability and longer training times. Nevertheless, the proposed methodology could be expanded to account for other types of antenna performance metrics, such as when different antenna families are of interest or when larger terminals are being considered.

The prediction problem is here reformulated as a regressive problem aimed at modeling the relationship between the space available for the antenna in a compact IoT terminal and the best bandwidth and efficiency that an IFA occupying that space can achieve. Towards this end, a Machine Learning (ML) algorithm is trained using data from numerical antenna designs which have been optimized with respect to the antenna performance criteria that are intended to be predicted. Such an approach differs from the existing theoretical ones, which can certainly provide an useful physical insight of the problem, but also generally rely on assumptions that are hard to fulfill in the real life (e.g., spherical geometries, ideal materials, optimal currents, etc.). In this work, the input data of the ML algorithm are obtained from simulated antenna designs that consider the constraints of practical implementations, such as lossy dielectric materials, lossy metals, specific feeding configurations, etc. The result is that the predicted maximum achievable bandwidth and efficiency values for an IFA reflects these practical aspects and gives therefore a more accurate idea of the antenna performance that should be targeted during the design process. As a consequence, the predicted maximum achievable bandwidth and efficiency values represents a useful metric for assessing the quality of terminal-integrated antenna solutions.

We would like to point out that we intentionally decided to use the expression "maximum achievable performance" instead of "performance bounds" or "performance limits". These latter are indeed clearly associated with the theoretical bounds (discussed above) that, by their mathematical definition, cannot be exceeded. In this paper, we rather propose to predict ~~estimate~~ the maximum achievable antenna bandwidth and efficiency using an ML approach. This prediction can, at least theoretically, be exceeded as it depends on the quality of the training dataset, that is, a limited (albeit large) number of manually-optimized antenna designs.

ML has already been used for different electromagnetic (EM) problems, as it has the potential to solve complex non-linear challenges by learning from the available data. The data-centric approach of ML allows getting close to the practical and real nature of the problem without requiring the approximations typical of analytical approaches. An overview of ML applied to electromagnetics, including communication, radar, and sensing is available in [19].

ML has been profitably used to address several electromagnetic problems, such as target reconstruction in biomedical imaging [20], layout definition of adaptive and reconfigurable antenna arrays [21], exposure prediction in 5G over

C-Band frequencies [22], or antenna near-field prediction [23]. However, the main domain of application of ML in electromagnetics is antenna geometry design and synthesis [24], [25]. In [26], a Bayesian regularization algorithm is utilized as the learning process for neural networks in the design of planar inverted-F antennas (PIFAs). The design optimization of a pattern-steerable varicap diode-loaded microstrip antenna has been addressed in [27]. More in detail, using a Multi-Layer Perceptron (MLP) model in conjunction with the Differential Evolution Algorithm (DEA), the work focused on enhancing return loss characteristics. In [28], a Support Vector Regression Machine (SVRM) and a metaheuristic Honey Bee Mating Optimization (HBMO) algorithm have been used to optimize the design of Frequency Selective Surface (FSS) for Ultra-Wide Band (UWB) Vivaldi antennas. The work in [29] explored the use of a Design Variable Surrogate Model (DVSM), where AutoEncoders (AEs) cascaded with Support Vector Regression (SVR) are employed to predict antenna design variables for various performance metrics while considering constraints on the operating frequency. In [30], the geometry of a compact monopole antenna with dual-band frequency reconfigurability, designed specifically for LoRa IoT applications, is optimized with various supervised regression machine learning models. Finally, [31] introduced a Machine-Learning-Assisted Optimization (MLAO) method for the design of pixelated and normalized Gaussian network (NGnet) generated antenna geometries.

All these works are summarized in Tab. 1 and compared to our work according to the ML algorithm which is used and the problem to be solved. Differently from all the previous works, our approach is novel in the electromagnetic problem that is addressed. To the best of our knowledge, this is the first time an ML-based approach is proposed to solve the problem of predicting maximum achievable antenna performance. Yet, our approach is limited as it considers specific antenna performance criteria (bandwidth and total efficiency) as well as a specific antenna configuration (terminal-integrated IFAs). However, the proposed methodology could be generalized to different antenna configurations (e.g. PIFA) and other types of performance metrics.

To avoid any misunderstanding, it is worth stressing that, in this work, the ML algorithm is neither used as a tool for designing antennas, nor as a way to find an optimal design of a specific IFA. The ML algorithm is here proposed as a tool to model the relation between the space available for the antenna in an certain IoT terminal, and the maximum bandwidth and total efficiency that an IFA occupying that space can achieve. In other words, the proposed approach will help the IFA designer to (a) *a-priori* know which performance could be achieved given the space dedicated to the antenna in a given terminal, or (b) *a-posteriori* benchmark the quality of a terminal-integrated IFA he already designed compared to the maximum performance that could have been achieved given the space dedicated to the antenna and the terminal size that he had at his disposal.

This article expands, improves, and completes the preliminary work presented in [32], explaining in detail the antenna optimization procedure used in the training set generation process, discussing the ML algorithm, and presenting the experimental validation. The main contributions of this work are:

- The creation of a dataset of terminal-integrated IFAs that have been simulated taking into account practical constraints and optimized in terms of impedance matching.
- The development of an ML-based approach for the prediction of the maximum achievable bandwidth and total efficiency, thus including the contribution of the mismatching losses, of terminal-integrated IFAs. Predictions can be used as a practically achievable target during the antenna design process or as a metric to assess the quality of already-designed antenna solutions.
- The proposed prediction approach has been validated at four different levels: through the evaluation of ML-related metrics, through the comparison with numerical results obtained from a commercial electromagnetic simulator, through the comparison with experimental measurements performed on different prototypes, and finally, through the comparison with theoretical results available in the literature.

This paper is organized as follows. In Sect. II, the ML-based model for the prediction of the maximum achievable bandwidth and total efficiency of terminal-integrated IFAs is presented. The results using the proposed ML-based approach when applied to different antenna-terminal configurations are presented in Sect. III. These results are experimentally validated and then compared with the state-of-the-art. Finally, some conclusions and perspectives are drawn in Sect. IV.

II. ML-based Approach for the Prediction of Maximum Achievable Antenna Bandwidth and Total Efficiency

The proposed ML-based prediction approach (described in detail in the following) has been applied to a specific antenna design test case, i.e., meander IFAs integrated into compact IoT terminals. The performance parameters to be predicted are the antenna total efficiency η and the fractional bandwidth F_{BW}. This latter is computer for $|S_{11}| \leq -6$ dB, a criterion that is enough for the antenna to be considered matched in many applications, and in particular in dealing with compact IoT terminals [33]. Total efficiency and fractional bandwidth are the two metrics that are of primary importance when dealing with IoT applications.

The proposed approach consists of 2 main phases: (A) building a dataset of optimized antenna-terminal configurations, and (B) training the model using this dataset.

TABLE 1. ML approaches used to solve electromagnetic problems

Ref.	EM Problem	ML Algorithm
[19]	Communication, radar, and sensing.	Various ML Approaches (Review Papers)
[20]	Reconstruction in biomedical imaging.	
[21]	Arrays layout definition.	
[22]	Exposure prediction.	Radial Basis Function Networks (RBFN), Exact-RBFNN and Generalized Regression Neural Networks (GRNN)
[23]	Antenna Near-Field prediction.	Convolutional Neural Networks (CNN), Near-Field Neural Network (Nef-Net)
[24]	Antenna geometry design and synthesis.	Various ML Approaches (Review Papers)
[25]		
[26]		Bayesian Regularization (BR)
[27]		Multi-Layer Perceptron (MLP)
[28]		Support Vector Regression Machine (SVRM), Honey Bee Mating Optimization (HBMO)
[29]		Design Variable Surrogate Model (DVSM), AutoEncoders (AEs), Support Vector Regression (SVR)
[30]		Gaussian Process Regression (GPR)
[31]		CNN, GPR
Our Work	**Maximum achievable antenna performance prediction.**	**MLP**

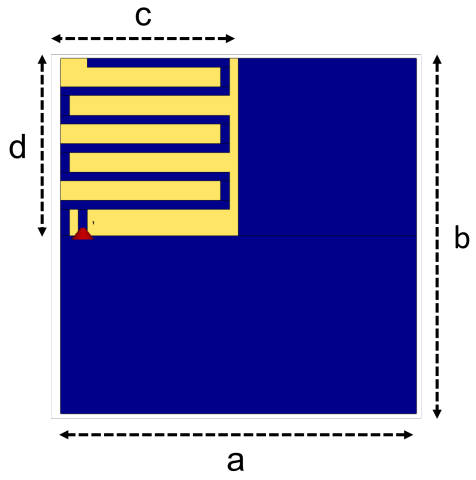

FIGURE 1. The selected antenna-terminal test case: a printed meander IFA located in the top-left corner of a terminal PCB.

A. Phase A: dataset creation.

The antenna-terminal test case considered in this work is a printed meandered IFA that fully occupies a dedicated space of dimension $c \times d$ located in the top-left corner of a terminal PCB of size $a \times b$, as shown in Fig. 1. All the metallic parts (in blue) are printed on a low-cost FR4 substrate (in yellow) of thickness 0.8 mm, dielectric constant $\epsilon_r = 4.3$, and loss tangent $\tan\delta = 0.025$. The remaining part of the PCB is fully covered by annealed copper (thickness of 0.035 mm), simulating the terminal electronic circuits and components, and acting as the ground plane for both the antenna and the electronics.

This specific structure has been chosen since it represents a typical antenna configuration for most modern compact wireless IoT devices. It is indeed a low-cost and easy-manufacturing solution [34], [35]. This allows the proposed approach to be immediately used as a benchmarking tool for the majority of the industrial terminal-integrated antenna solutions available today. Moreover, using an IFA structure facilitates the antenna electric behavior optimization. As a matter of fact, the resonant frequency can be easily controlled by varying the length of the IFA electrical length (meander lines), while the impedance matching at the resonance can be maximized by tuning the distance between the IFA feeding point and the short-circuit.

Phase A of the proposed approach is pictorially represented in Fig. 2. The dataset to be used by the ML algorithm has been created by varying the space available for the terminal (a, b) and the antenna dimensions (c, d) as shown in Tab. 2. Moreover, the following constraints have been considered: $a \neq c$, $b \neq d$, and at least 5 mm of ground plane between the edge of the terminal and the antenna's dedicated space is guaranteed. Finally, a set of $S = 576$ antenna-terminal combinations is obtained.

The variable ranges in Tab. 2 have been chosen because they encompass the dimensions of typical compact IoT devices. For example, considering the operating frequency of 868 MHz (the most commonly used frequency band in IoT applications), these selected ranges approximately include terminals whose sizes go from 40×40 mm^2 to 60×80 mm^2. Considering wider ranges of variables would include in the study larger IoT terminals. The maximum achievable performance of antennas integrated in these terminals will naturally increases to very high values (e.g., because of the presence of a larger ground plane) and consequently their

This article has been accepted for publication in IEEE Open Journal of Antennas and Propagation. This is the author's version which has not been fully edited and content may change prior to final publication. Citation information: DOI 10.1109/OJAP.2024.3487498

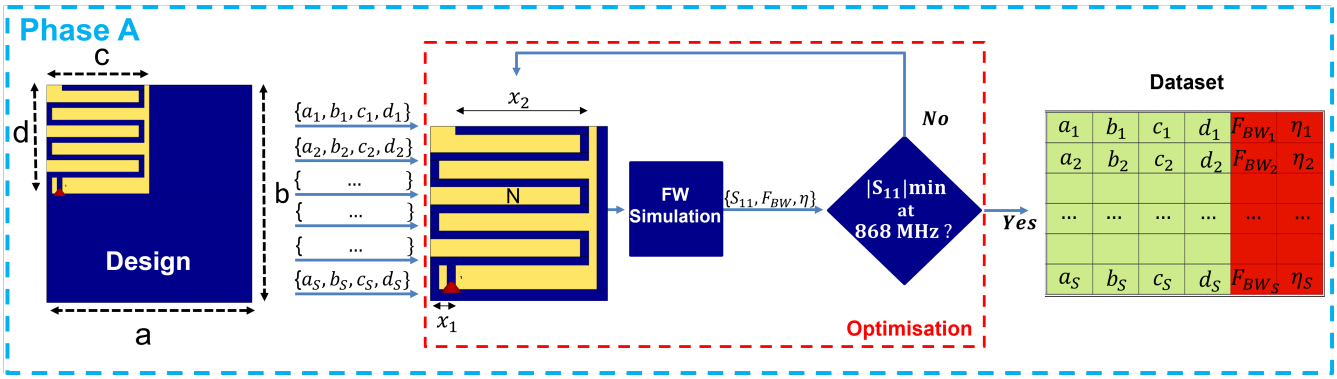

FIGURE 2. Pictorial representation of the proposed ML-based prediction approach. Phase A: dataset creation.

TABLE 2. Geometrical variations to create the ML dataset.

Param.	Minimum (λ)	Maximum (λ)	Step (λ)
a	0.12	0.18	0.015
b	0.12	0.24	0.030
c	0.06	0.12	0.015
d	0.06	0.12	0.015

TABLE 3. Meander IFA's fixed geometrical parameters.

Param.	Value (mm)	Description
x_3	1	Width of the printed lines
x_4	3	Length of the shorting line
x_5	2.5	Length of the feeding line
x_6	1	Distance between IFA and ground plane

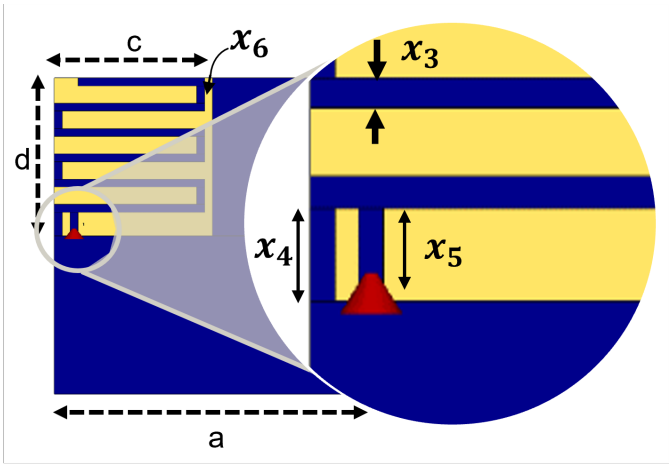

FIGURE 3. Fixed geometrical parameters of the terminal-integrated meandered IFA.

TABLE 4. The dataset.

s	$a(\lambda)$	$b(\lambda)$	$c(\lambda)$	$d(\lambda)$	$F_{BW}(\%)$	$\eta(\%)$
1	0.12	0.12	0.05	0.05	1.8	39.46
2	0.135	0.12	0.05	0.05	2.03	42.3
3	0.15	0.12	0.05	0.05	2.1	44.6
4	0.165	0.12	0.05	0.05	2.03	46.9
5	0.18	0.12	0.05	0.05	2.02	49.8
6	0.12	0.15	0.05	0.05	2.07	42.96
7	0.135	0.15	0.05	0.05	2.1	44.67
...	...	...	...	...	...	...
26	0.12	0.12	0.05	0.0675	2.2	36.05
...	...	...	...	...	...	...
576	0.18	0.24	0.12	0.12	2.6	38.3

prediction, which is the objective of this work, will be less interesting.

For each (a, b, c, d) combination, the IFA geometry has been manually optimized with the aim of minimizing the $|S_{11}|$ parameter at the operating frequency of 868 MHz. The optimization process has been carried out through a manual parametric study on the feed-short distance x_1, the length of the IFA's last meander x_2, and the number of meanders N (Fig. 2). All the remaining geometrical parameters have been kept fixed to the values reported in Tab. 3. With reference to Fig. 3, x_3 is the width of all the printed lines, x_4 is the length of the shorting line, x_5 is the length of the feeding line, and x_6 is the distance between the IFA's edge and the ground plane in the width direction. The feeding point is indicated with a red arrow.

All the simulations have been carried out using the CST Studio Suite on an Intel i5-4460 3.00 GHz machine with 16 GB of RAM. The entire process, performed manually, took about 200 hours. 576 configurations of antenna-terminal dimensions (a, b, c, d) have been numerically modeled, simulated, and optimized. These configurations have been used to build the dataset for training the ML algorithm, where (a, b, c, d) are the input variables, and the simulated fractional bandwidth F_{BW} and the total efficiency η of the optimized solutions, are the labels (Tab. 4).

B. Phase B: ML model training

Phase B of the proposed approach is pictorially represented in Fig. 4.

1) The Multi-Layer Perceptron (MLP) Algorithm

From an ML perspective, the problem at hand is a multi-target regression problem, in which two continuous values

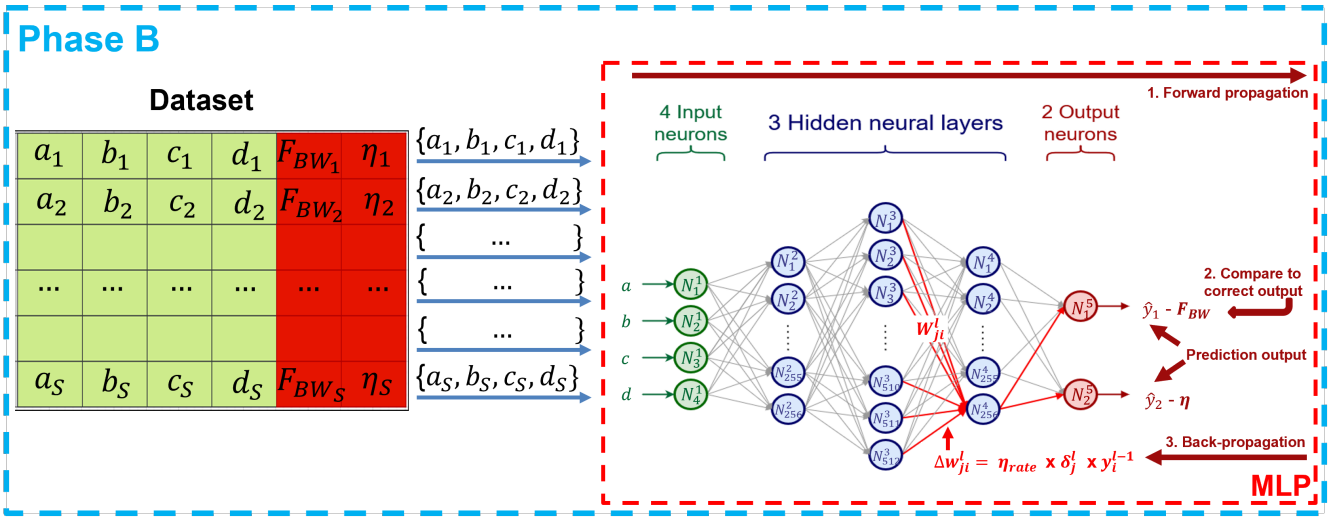

FIGURE 4. **Pictorial representation of the proposed ML-based prediction approach. Phase B: ML model training.**

(F_{BW} and η) must be predicted from a set of 4 inputs (a, b, c, d). To solve this regression problem [36], a Deep Neural Network (DNN) based on a Multi-Layer Perceptron (MLP) is used. An MLP is a commonly used supervised ML algorithm that has widely demonstrated its effectiveness during the last years. An MLP consists of an input layer, one or more hidden layers, and an output layer for the predictions. In each layer, there is a number of neurons called Perceptrons.

In the input layer, the input neurons only transmit the information to the first hidden layer. Between the layers, the neurons are fully connected via synapses, where every synaptic weight is updated during the training phase. Every neuron performs the sum of the products between its inputs and the corresponding synaptic weights (plus a bias), followed by a non-linear activation function to produce its output.

As shown in Fig. 4, the MLP model adopted in this work is composed of an input layer with 4 neurons corresponding to the 4 input dimensions (a, b, c, d), a certain number of hidden layers (3 in Fig. 4), and an output layer composed of 2 neurons is used for the F_{BW} and η performance predictions.

2) Hyperparameter Selection

The training process is driven by a set of hyper-parameters (HPs). These are critical settings that can greatly influence how well the algorithm performs [37]. In our case, the HPs are: the optimization function, the activation function, the Loss Function (LF), the number of hidden layers as well as the number of neurons per hidden layer.

Concerning the optimization function, the Adaptive Moment Estimation (ADAM) function has been used. Thanks to its robustness and efficiency, this is a popular solution used in machine learning for training deep learning models. It combines the advantages of two other extensions of Stochastic Gradient Descent (SGD): the Adaptive Gradient Algorithm (AdaGrad) and the Root Mean Square Propagation (RMSProp). The steps of the ADAM optimization algorithm are detailed in [38]. The convergence properties of the ADAM function depend on the Learning Rate (LR) parameter [39]. In our work, this parameter has been fixed as default to 0.001, as suggested in [38].

Regarding the non-linear activation function, the widely used Rectified Linear Unit (ReLU) has been adopted [40], [41]. The ReLU activation function outputs the input directly if it is positive; otherwise, it outputs zero. It has several advantages that make it popular in deep learning. First, despite being simple, ReLU introduces non-linearity into the model, allowing it to learn complex patterns. Then, the ReLU function is computationally efficient as it involves simple thresholding at zero. Finally, ReLU activation leads to sparse activation, meaning that only a few neurons are activated at the same time, which can improve the efficiency of the network.

As LF, we have computed the Mean Square Error (MSE) between the predicted and the actual values. This is a common metric to assess the performance of the trained model in regression problems. The MSE is computed as follows:

$$MSE = \frac{1}{n}\sum_{i=1}^{n}(y_i - \hat{y}_i)^2 \tag{1}$$

where n is the number of training samples, y_i is the actual value obtained by simulation from CST Studio Suite, and $\hat{y}_i$ is the predicted value. The MSE loss function is widely used due to its simplicity and the fact that it is differentiable, which is important for optimization algorithms such as the gradient descent. Compared to the MAE loss function, another common metrics in regression problems, the MSE function improves the convergence speed and the accuracy of the model [42].

Concerning the number of hidden layers, and the number of neurons per hidden layer, they have been varied to find the

This article has been accepted for publication in IEEE Open Journal of Antennas and Propagation. This is the author's version which has not been fully edited and content may change prior to final publication. Citation information: DOI 10.1109/OJAP.2024.3487498

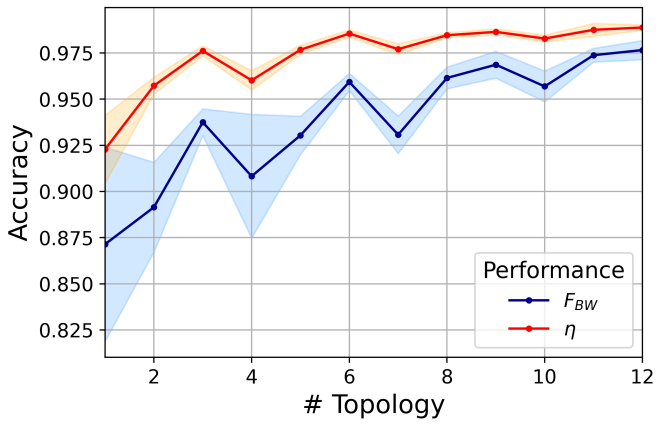

FIGURE 5. Test accuracy of the ML model for the different MLP topologies listed in Tab. 5.

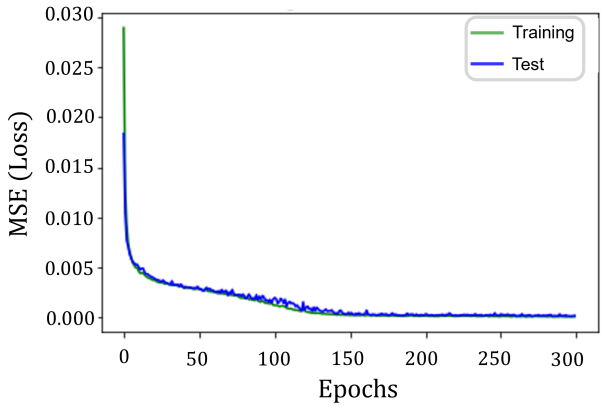

FIGURE 6. Variation over the epochs of the MSE for topology #6 on training and test data.

best trade-off between the dimension of the neural network and the predicted accuracy. This study is discussed in the next section.

3) MLP Training Process

The available dataset has been divided into training and test datasets. The 80/20 training/test dataset ratio has been shown to be empirically optimal [43], and it is, in fact, the most commonly used in ML. However, for the sake of completeness, this ratio has been varied and the results obtained are discussed in the next section. Considering the small size of the dataset, 10% of the samples were used during the training for the validation. A cross-validation was performed with a $K - Fold$ method (with K=5) [44] to ensure robust evaluation of the model by splitting the dataset into five subsets. Each subset at a time is used as the test set, while the remaining four subsets form the training set.

The MLP training algorithm [45] used in this work is the gradient descent with Back-Propagation (BP). It is a supervised off-line learning algorithm [46]. TensorFlow Keras API [47] has been used for defining and training the MLP model. To train the MLP model, the gradient (ΔW_{ji}^l) of the MSE (loss) between the desired output (i.e., the label) and the prediction is computed. Then, the synaptic weights are updated according to this gradient. The objective of the back-propagation algorithm is to minimize the loss. The synaptic weights are updated as follows:

$$W_{ji}^l(t+1) = W_{ji}^l(t) + \eta_{rate} \times \delta_j^l(t) \times y_i^{l-1}(t) \qquad (2)$$

where t is the learning iteration index, η_{rate} is the learning rate, δ_j^l is the error gradient in the layer l of the neuron j, and y_j^{l-1} is the output in the layer l of the neuron j. Moreover, for the hidden layers,

$$\delta_j^l(t) = f'(s_j^l(t)) \times \sum_{k=0}^{N_{l+1}} \delta_k^{l+1}(t) \times W_{jk}(t) \qquad (3)$$

f' being the derivative of the activation function f, while for the output layer,

$$\delta_j^l(t) = f'(s_j^l(t)) \times e_j^l(t) \qquad (4)$$

where e_j^l represents the error, i.e., the difference between the prediction and the ground truth in the layer l of the neuron j.

This process (illustrated in Fig. 4) is repeated through the training dataset for 300 epochs. It is expected that, at the end of the training, the MLP can approximate the complex function which links the inputs to the outputs.

TABLE 5. Characteristics of the different MLP topologies and corresponding accuracy values.

	MLP Topologies		Accuracy	
#	Number of TP	Hidden Layers	F_{BW}	η
1	218	8-16	87.1%	92.3%
2	2 402	32-64	89.1%	95.7%
3	34 178	128-256	93.8%	97.6%
4	1 186	16-32-16	90.8%	96%
5	17 026	64-128-64	93%	97.7%
6	264 706	256-512-256	95.9%	98.6%
7	8 578	32-64-64-32	93.1%	97.7%
8	132 610	128-256-256-128	96.1%	98.5%
9	2 103 298	512-1024-1024-512	96.9%	98.6%
10	82 946	64-128-256-128-64	95.7%	98.3%
11	1 314 818	256-512-1024-512-256	96.2%	98.6%
12	20 987 906	1024-2048-4096-2048-512	97.5%	98.8%

III. Results and Discussion

A. MLP topologies and training results.

The accuracy on both F_{BW} and η obtained with the training of different MLP topologies is shown in Fig. 5. Such topologies differ in dimensions or, more specifically, in the number of trainable parameters (TP), which depend

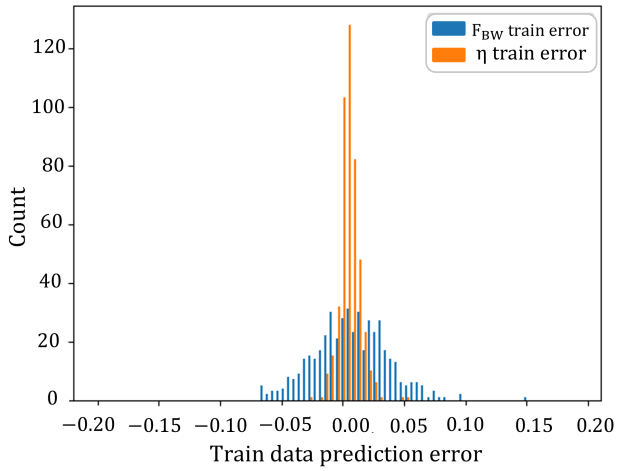

FIGURE 7. **Predictions errors on train dataset for Topology #6**

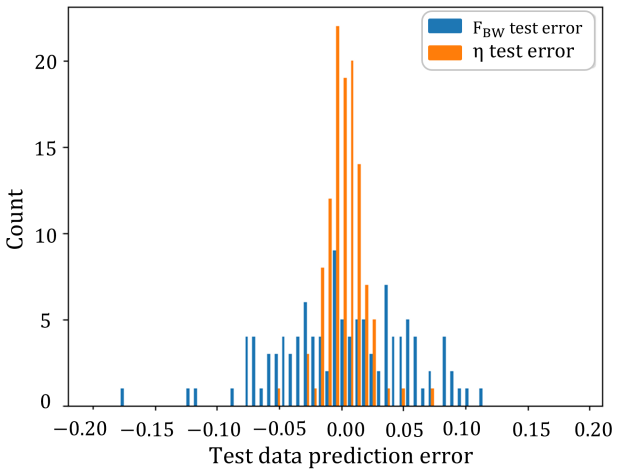

FIGURE 8. **Predictions errors on test dataset for Topology #6**

on the characteristics of the hidden layers. All the details are reported in Tab. 5. For all the topologies, the 80/20 traning/test dataset ratio has been considered.

The tested MLP topologies have from 2 to 5 hidden layers and different numbers of neurons per layer (third column in Tab. 5). To obtain statistically-significant results, the accuracy values are averaged over 10 runs (training processes) for each topology. The variance over the 10 runs is represented by the light-colored area charts in Fig. 5. As expected, the bigger the model, the better the accuracy. Moreover, the variance of the results clearly reduces as the dimension of the network increases. However, topology #6 represents a good trade-off between the number of trainable parameters, and thus the time and computational resources needed for the training process, and the accuracy. This latter is about 95.9% and 98.6% according F_{BW} and η respectively. All the results reported in the remaining part of the paper have been obtained using this topology.

Successively, the performance of the prediction model using the selected topology has been evaluated for different training/test ratios. As for the topology study discussed above, to obtain statistically-significant results, the accuracy values are averaged over 10 training runs. As shown in Tab. 6, the obtained results indicate that the 80/20 ratio is effectively the one providing the best prediction accuracy. The average (over 10 runs) accuracy is 95.9% for the bandwidth F_{BW} and 98.6% for the total efficiency η. The standard deviations are only 0.47% and 0.20% for F_{BW} and η, respectively. All the results reported in the remaining part of the paper have been obtained using this training/test dataset ratio. Reminding that the entire available dataset consists of 576 samples, the 80/20 ratio determines a training set of 461 samples and a test set of 115 samples. The validation set, being 10% of the training set, consists of 46 samples.

The MSE (loss) against the number of epochs for topology #6 and for the 80/20 training/test dataset ratio is shown in Fig. 6. As can be observed, the validation loss on test data is very close to the training loss. This shows that the algorithm is able to learn from the data without overfitting. It also illustrates its ability to generalize with respect to new data.

Figs. 7 and 8 show the prediction errors, in the form of histograms, for the train and the test data respectively. To be able to compare F_{BW} and η results, the errors (x-axis) have been normalized with respect to the actual values. As expected, slightly larger errors can be found for the test data (Fig. 8) compared to the training data (Fig. 7). More importantly, the variability of the error on the fractional bandwidth F_{BW} is higher than the one on the total efficiency η. This could indicate that a larger number (more the 576) of training samples are needed to obtain more accurate predictions of F_{BW}.

B. F_{BW} and η predictions for unknown antenna-terminal configurations.

Once trained, the ML model is used to predict the maximum achievable fractional bandwidth F_{BW} and total efficiency η of terminal-integrated IFAs. Predictions are performed for several combinations of terminal and antenna space dimensions, which are unknown to the ML algorithm. These predictions are shown through color maps in Figs. 9 and 10. Color maps are indeed relevant to rapidly visualize and analyze the predicted performance for each antenna-terminal configuration.

For each color map, the horizontal and vertical dimensions of the terminal (a and b) have been fixed to specific values within the ranges $a = \{0.135, 0.15, 0.165, 0.18\}\lambda$ and $b = \{0.15, 0.18, 0.21, 0.24\}\lambda$, respectively, while the dimensions of the space available for the antenna (c and d) are varied between 0.05λ and 0.12λ. Consequently, moving from bottom-left to top-right in Figs. 9 and 10 consists in considering larger terminal dimensions, while moving from

This article has been accepted for publication in IEEE Open Journal of Antennas and Propagation. This is the author's version which has not been fully edited and content may change prior to final publication. Citation information: DOI 10.1109/OJAP.2024.3487498

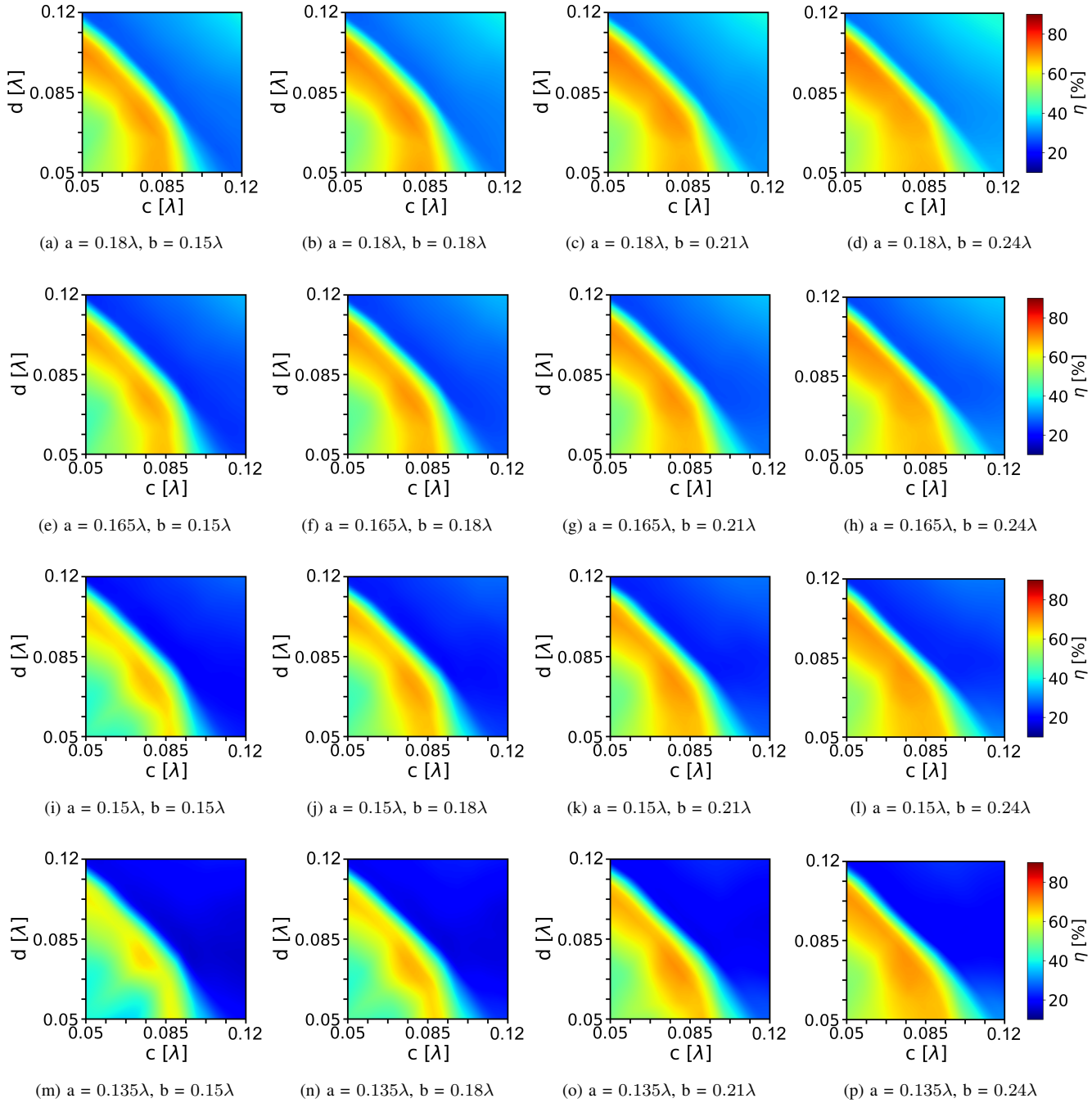

(a) a = 0.18λ, b = 0.15λ (b) a = 0.18λ, b = 0.18λ (c) a = 0.18λ, b = 0.21λ (d) a = 0.18λ, b = 0.24λ

(e) a = 0.165λ, b = 0.15λ (f) a = 0.165λ, b = 0.18λ (g) a = 0.165λ, b = 0.21λ (h) a = 0.165λ, b = 0.24λ

(i) a = 0.15λ, b = 0.15λ (j) a = 0.15λ, b = 0.18λ (k) a = 0.15λ, b = 0.21λ (l) a = 0.15λ, b = 0.24λ

(m) a = 0.135λ, b = 0.15λ (n) a = 0.135λ, b = 0.18λ (o) a = 0.135λ, b = 0.21λ (p) a = 0.135λ, b = 0.24λ

FIGURE 9. Color maps for η predictions.

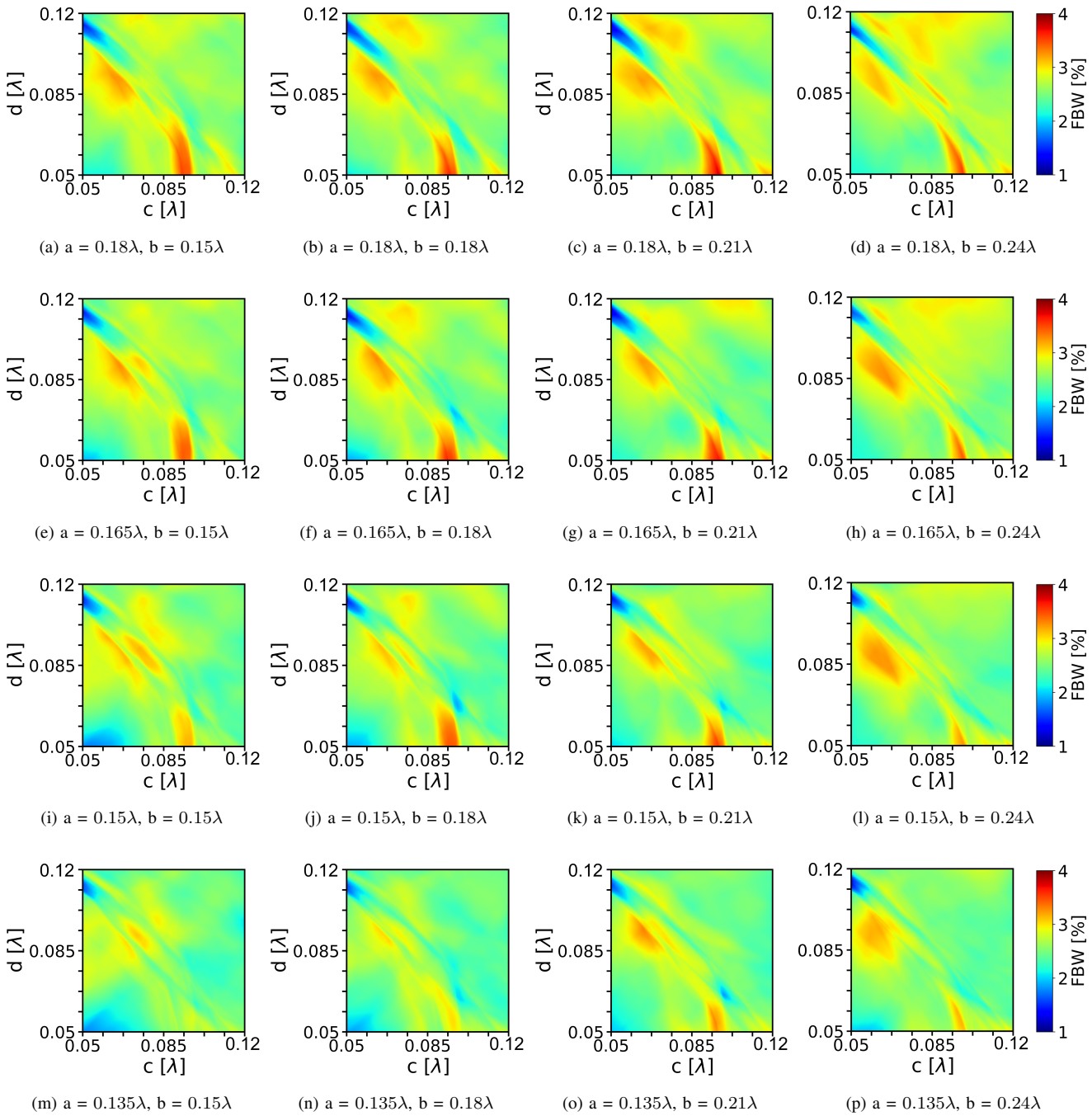

(a) a = 0.18λ, b = 0.15λ (b) a = 0.18λ, b = 0.18λ (c) a = 0.18λ, b = 0.21λ (d) a = 0.18λ, b = 0.24λ

(e) a = 0.165λ, b = 0.15λ (f) a = 0.165λ, b = 0.18λ (g) a = 0.165λ, b = 0.21λ (h) a = 0.165λ, b = 0.24λ

(i) a = 0.15λ, b = 0.15λ (j) a = 0.15λ, b = 0.18λ (k) a = 0.15λ, b = 0.21λ (l) a = 0.15λ, b = 0.24λ

(m) a = 0.135λ, b = 0.15λ (n) a = 0.135λ, b = 0.18λ (o) a = 0.135λ, b = 0.21λ (p) a = 0.135λ, b = 0.24λ

FIGURE 10. Color maps for F_{BW} predictions.

TABLE 6. Training/Test set ratio comparison and achieved ML performance.

Training/Test Ratio [%]	Number of Samples		ML Performance [%]			
	Train	Test	$\text{FBW}_{Accuracy}$	FBW_{std}	$\eta_{Accuracy}$	η_{std}
90/10	518	58	94.6	0.95	94.2	0.59
70/30	403	173	94.5	0.66	91.8	0.78
80/20	461	115	95.9	0.47	98.6	0.20

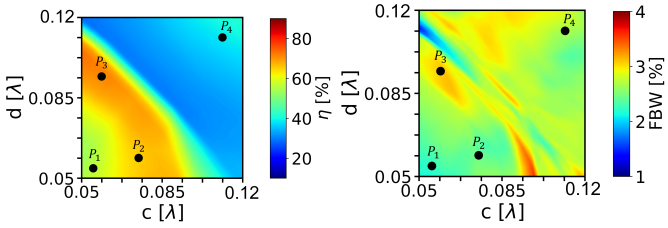

(a) (b)

FIGURE 11. The selected 4 antenna-terminal configurations for the comparison with numerical and experimental results. The points representing these configurations are shown on the (a) η and (b) F_{BW} color maps for a terminal size of $0.18\lambda \times 0.24\lambda$.

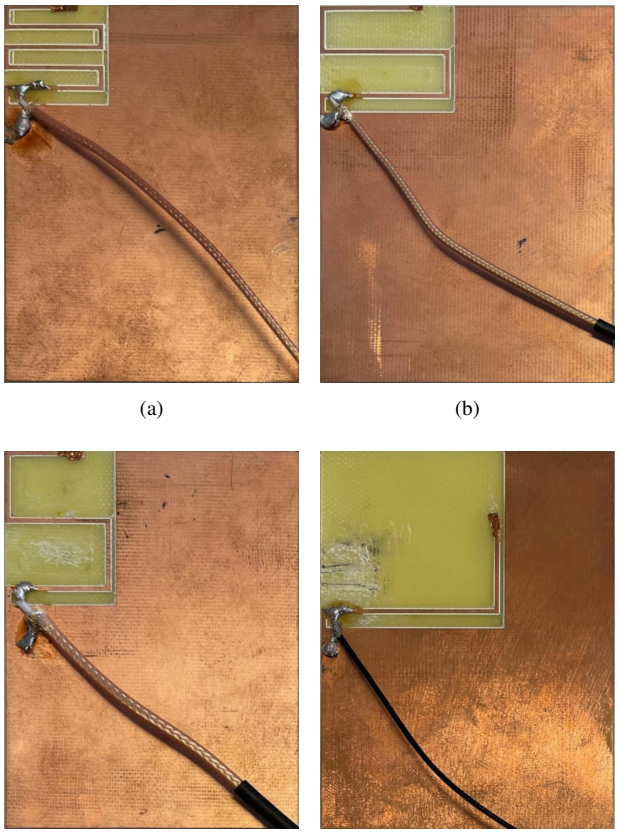

(a) (b) (c) (d)

FIGURE 12. Prototypes of the selected 4 antenna-terminal configurations: (a) P_1, (b) P_2, (c) P_3, and (d) P_4.

bottom-left to top-right inside a color map means a larger antenna space within a specific terminal PCB.

Concerning the color maps for the predictions of the total efficiency η (Fig. 9), it can be clearly observed that, whatever the terminal size, the predicted maximum achievable performance exhibits the same variation trend. As the space available for the antenna increases (going from bottom-left to top-right on the color maps), the maximum achievable total efficiency increases up to a region with the highest values, which is followed by a fast drop towards minimum values. The area with the highest values is approximately the same in all the color maps. This indicates that the antenna space that allows for the highest efficiency is the one given by $c \sim 0.075\lambda$ and $d \sim 0.075\lambda$, independently of the terminal size. Such an antenna space corresponds to about 28% of the PCB surface when the terminal is small (e.g., $a = 0.135\lambda$ and $b = 0.15\lambda$), while it decreases to around 13% when the terminal is bigger (e.g., $a = 0.18\lambda$ and $b = 0.24\lambda$). On the other hand, the shape of the region with the highest values, spanning along a slanted direction parallel to the bottom-right/top-left diagonal of the color map, indicates that, if one side of the space dedicated to the antenna is smaller than 0.075λ, the other side should be longer, and vice-versa.

It must be also pointed out that, despite the maximum achievable total efficiency is obtained only for a specific size of the space available for the antenna, such maximum value varies with the terminal dimensions. As it can be seen, when the terminal is very compact, as in Fig. 9(m) ($0.135\lambda \times 0.15\lambda$), the maximum achievable total efficiency is about 57%, while it increases to about 75% when a $0.18\lambda \times 0.24\lambda$ terminal is considered, as shown in Fig. 9(d).

Concerning the color maps for the maximum achievable bandwidth predictions (Fig. 10), it can be observed that, no matter the size of the terminal, the variation of the predicted F_{BW} is limited, with values approximately going from 1.5% to 3.5%. In other words, the choice of a specific combination of antenna and terminal space dimensions has a much higher impact on the efficiency than the bandwidth. Obtaining larger operational bandwidth would probably require (a) further enlarging the terminal and the antenna space dimension (going beyond the values considered in this study), or (b)

TABLE 7. Comparison between CST simulations, ML predictions, and prototypes measurements for the selected antenna-terminal configurations.

P_t	Antenna-Terminal Configurations $[\lambda]$				Performance [%]						Pred.-CST Difference	
	a	b	c	d	F_{BW}			η			ΔBW @-6dB	$\Delta\eta$
					CST	Pred	Meas	CST	Pred	Meas	MHz	%
1	0.18	0.24	0.054	0.054	3.53	1.94	4.03	62.38	58.47	58.88	13.80	3.91
2	0.18	0.24	0.075	0.058	4.20	2.35	4.75	66.83	66.49	66.68	16.05	0.34
3	0.18	0.24	0.058	0.093	4.26	3.27	3.99	68.37	69.46	69.18	8.59	1.09
4	0.18	0.24	0.110	0.110	2.40	2.57	2.97	36.78	38.10	38.37	1.47	1.32

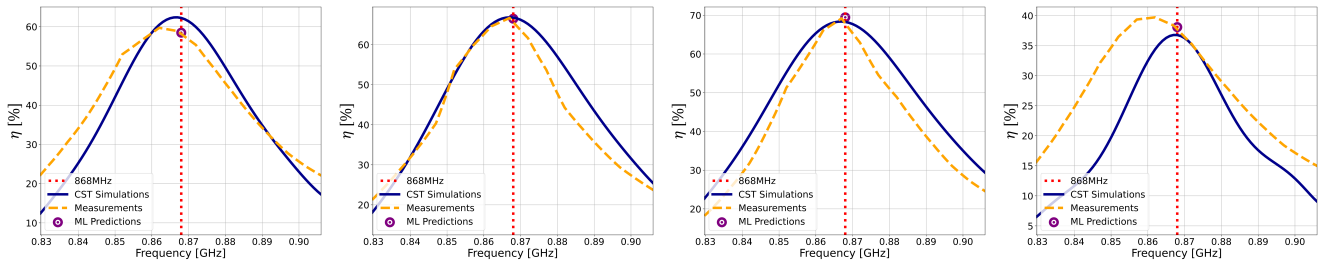

(a) (b) (c) (d)

FIGURE 13. Comparison between ML predictions, simulations (CST), and measurements for the 4 selected antenna-terminal configurations: total efficiency η results for (a) P_1, (b) P_2, (c) P_3, and (d) P_4.

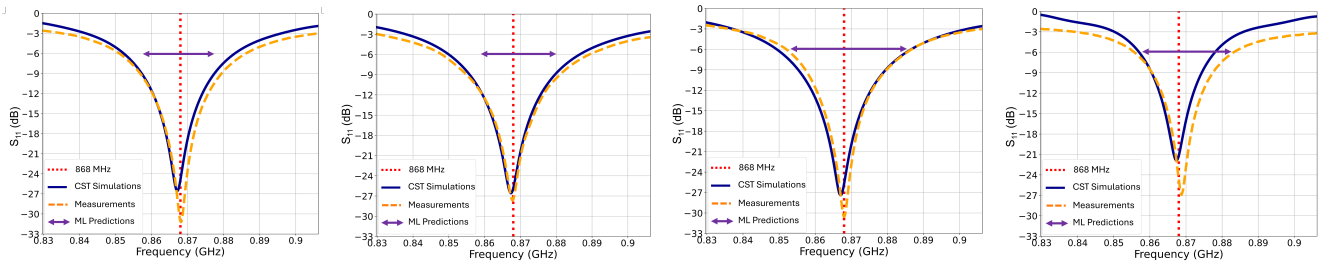

(a) (b) (c) (d)

FIGURE 14. Comparison between ML predictions, simulations (CST), and measurements for the 4 selected antenna-terminal configurations: fractional bandwidth F_{BW} results (in terms of S_{11}) for (a) P_1, (b) P_2, (c) P_3, and (d) P_4.

completely changing the antenna geometry, moving from meandered IFAs to other antenna families.

C. Comparison of ML predictions with simulated and experimental results.

In order to validate the predictions provided by the ML model, a comparison with results obtained through numerical simulations and experimental measurements has been performed for 4 different combinations of the antenna-dedicated space and the terminal dimension.

The selected combinations are represented by the 4 points $P_t, t = 1, 2, 3, 4$ reported on the color maps in Fig. 11. These points correspond to antenna-terminal configurations in which the terminal size is fixed to $0.18\lambda \times 0.24\lambda$, while the space available for the antenna varies according to the values of (c, d) reported in Tab. 7 and detailed as follows:

- $P_1 : c = d$ with the antenna space being about 15% of the terminal,
- $P_2 : c > d$ with $c \approx 1.3 \times d$.
- $P_3 : c < d$ with $c \approx 0.6 \times d$.
- $P_4 : c = d$ with the antenna space being about 30% of the terminal.

It is worth reminding that these 4 configurations have never been seen by the ML algorithm during the training phase.

The numerical validation of the predicted maximum achievable bandwidth and total efficiency has been carried out as follows. For each P_t configuration, the corresponding antenna-terminal structure (shown in Fig. 1) has been modeled using CST Microwave Studio. The geometrical parameters of the IFA have been automatically optimized using the Particle Swarm Optimizer (PSO) available in CST with the objective of minimizing the $|S_{11}|$ at 868 MHz.

Given the small number of parameters to be optimized (x_1, x_2 and N), and letting the optimization procedure stop after a very large number of iterations (1000), the PSO should guarantee the best antenna solution or, in other words, the one exhibiting the performance closer to the maximum achievable bandwidth and total efficiency for a terminal-integrated IFA. Successively, for the experimental validation, the optimized antennas have been realized (Fig. 12) and measured in a SATIMO Starlab station.

The comparison between CST numerical simulations, the predicted values from the ML model, and the experimental measurements from prototypes is shown in Figs. 13 and 14 and detailed in Tab. 7. The predicted results are averaged over 10 runs. In general, it can be noticed that the simulated results are in good agreement with the measured ones, with some slight differences that can be ascribed to imperfections in the realization of the prototypes. Concerning the total efficiency η, the CST simulated results are close to the ML predictions, the difference being less than 4% whatever the configuration (last column in Tab. 7 and Fig. 13). For the F_{BW}, the difference is only a few MHz for P_3 (8.59 MHz) and P_4 (1.47 MHz), while it becomes larger (about 15 MHz) for P_1 and P_2 (penultimate column in Tab. 7 and Fig. 14). This increase indicates that the ML model has more difficulty in providing accurate bandwidth predictions when the space dedicated to the antenna is small with respect to the terminal dimension (bottom-left region in Fig. 11(b)). This behavior is in agreement with the larger variability of the error on F_{BW} shown in Figs. 7 and 8. A possible solution would be to increase the number of epochs considered in the training phase. However, this would probably cause the model to overfit because of the small size of the available dataset. To avoid that, the size of the training set should be increased (mainly by including more samples characterized by limited antenna dedicated spaces). This will improve the maximum achievable bandwidth prediction accuracy without the overfitting risk.

D. Comparison of ML-based F_{BW} predictions with a theoretical approach [48]

In this section, the F_{BW} predictions obtained using the proposed ML model are compared with the results of a theoretical approach available in the literature.

In [48], the objective was to find the optimal bandwidth according to the position of the antenna dedicated space for a terminal-antenna fixed configuration: $a = 0.15\lambda$ mm, $b = 0.15\lambda$ mm, $c = 0.06\lambda$ mm, and $d = 0.06\lambda$, considering an operating frequency at 900 MHz. The authors highlighted that a meander antenna placed at a corner of the terminal is the best position for bandwidth maximization. According to [48] (see Fig. 9 in [48]), the best possible fractional bandwidth for an optimized planar meander antenna is 4.6%, for a reflection coefficient at -3 dB. In order to re-scale this result for a reflection coefficient of -6 dB, i.e. the one considered in the proposed ML-based approach, eq. (14) from [48] can be used as follows:

$$FBW_2 \approx FBW_1 \frac{|\Gamma_2|\sqrt{1-|\Gamma_1|^2}}{|\Gamma_1|\sqrt{1-|\Gamma_2|^2}} \tag{5}$$

FBW_2 being the desired threshold band, FBW_1 the actual threshold band (4.6%), $|\Gamma_2|$ the -6 dB reflection coefficient considered in this work, and $|\Gamma_1|$ the -3 dB reflection coefficient taken into account in [48]. The result is a new optimal fractional bandwidth of 2.53%.

The ML model has been executed for the terminal and antenna space dimensions specified in [48]. The prediction, reported in Tab. 8, is $F_{BW} = 2.69\%$. The difference with respect to [48] is only 0.16%, which represents 1.4 MHz of bandwidth at 868 MHz. Such a close agreement confirms the reliability of the predictions calculated by the proposed ML-based approach.

TABLE 8. Comparison with the results reported in [48].

	[48] [%]		**Our ML Model** [%]		**Error** [MHz]
F_{BW}	@-3dB	@-6dB	@-3dB	@-6dB	@-6dB
Results	4.60	2.53	4.53	2.69	1.4

IV. Conclusion

In this paper, a novel approach to predict the maximum achievable bandwidth and total efficiency performance of meander IFAs integrated in compact IoT terminals has been proposed. This approach is based on an MLP model that has been trained using data extracted from CST simulations for nearly 600 optimized antenna designs. These simulations allow us to take into account the constraints of practical implementations such as lossy materials and specific feeding configurations. The obtained results show that the proposed ML-based approach is able to predict with accuracy the maximum achievable fractional bandwidth and total efficiency of terminal-integrated IFAs. Once the ML model has been trained, these predictions can be obtained without time-consuming electromagnetic simulations. The effectiveness of the proposed approach has been validated through the analysis of ML-related metrics, through the comparison with numerical and experimental results, and through the comparison with theoretical results available in the scientific literature.

Future work will be focused on the following aspects. First of all, the use of a manual approach to generate the dataset for the ML algorithm is certainly not convenient. To overcome this issue, we are currently developing a Python script (that will be made available to the scientific community soon) to automatically generate a dataset of optimized IFA antenna geometries using CST Microwave Studio. Using this script, the time required is consistently reduced (as no interaction with the antenna designer is required) and, most

importantly, it can run autonomously, so that the time of the antenna designer remains available for other tasks. This will allow a more efficient generation of training samples so that the size of the dataset could be augmented.

Secondly, in order to generalize the proposed approach, additional printed antenna families will be considered. This will require adding more training data for the new antenna geometries as well as modifying the MLP topology to include another input neuron representing the antenna family.

Finally, the use of other types of ML algorithms, such as Convolutional Neural Networks (CNNs), will also be studied.

REFERENCES

[1] "State of IoT Summer 2024 report," IoT Analytics, 2024 [Online]. Available: https://iot-analytics.com/number-connected-iot-devices/

[2] "Cisco Annual Internet Report (2018–2023)," Cisco, White Paper, 2020 [Online]. Available: https://www.cisco.com/c/en/us/solutions/collateral/executive-perspectives/annual-internet-report/white-paper-c11-741490.html

[3] S. R. Best, "State-of-the-art in the design of electrically small antennas," in Proc. European Conference on Antennas and Propagation, Rome, Italy, pp. 2729-2732, 2011.

[4] H. A. Wheeler, "Fundamental Limitations of Small Antennas," Proc.IRE, vol. 35, no. 12, pp. 1479-1484, Dec. 1947, doi: 10.1109/JRPROC.1947.226199.

[5] L. J. Chu, "Physical limitations of omnidirectional antennas," J. Appl. Phys., vol. 19, pp. 1163-1175, 1948.

[6] R. Collin and S. Rothschild, "Evaluation of antenna Q," IEEE Trans. Antennas Propag., vol. 12, no. 1, pp. 23-27, Jan. 1964.

[7] J. S. McLean, "A re-examination of the fundamental limits on the radiation Q of electrically small antennas," IEEE Trans. Antennas Propag., vol. 44, no. 5, pp. 672-, May 1996.

[8] H. L. Thal, "New Radiation *Q* Limits for Spherical Wire Antennas," IEEE Trans. Antennas Propag., vol. 54, no. 10, pp. 2757-2763, Oct. 2006.

[9] M. Gustafsson, C. Sohl, and G. Kristensson, "Physical limitations on antennas of arbitrary shapes," Proc. R. Soc. A, vol. 463, pp. 2589–2607, 2007.

[10] A. D. Yaghjian and H. R. Stuart, "Lower Bounds on the Q of Electrically Small Dipole Antennas," IEEE Trans. Antennas Propag., vol. 58, no. 10, pp. 3114-3121, Oct. 2010.

[11] J. Chalas, K. Sertel, J.L. Volakis, "Computation of the Q Limits for arbitrary-shaped antennas using characteristic modes," IEEE Trans. Antennas Propag., vol. 64, no. 7, pp. 2637-2647, July 2016.

[12] L. Thal, "Q Bounds for Arbitrary Small Antennas: A Circuit Approach," IEEE Trans. Antennas Propag., vol. 60, no. 7, pp. 3120-3128, July 2012.

[13] M. Capek et al, "Evaluating radiation efficiency from characteristics currents," IET Microw. Antennas Propag., vol. 9, no.1, pp 1015, 2015.

[14] L. Jelinek and M. Capek, "Optimal Currents on Arbitrarily Shaped Surfaces," IEEE Trans. Antennas Propag., vol. 65, no. 1, pp. 329-341, Jan. 2017.

[15] M. Gustafsson, M. Capek and K. Schab, "Tradeoff Between Antenna Efficiency and Q-Factor," IEEE Trans. Antennas Propag., vol. 67, no. 4, pp. 2482-2493, April 2019.

[16] C. Pfeiffer, "Fundamental Efficiency Limits for Small Metallic Antennas," IEEE Trans. Antennas Propag., vol. 65, no. 4, pp. 1642-1650, April 2017.

[17] M. Shahpari and D. V. Thiel, "Fundamental Limitations for Antenna Radiation Efficiency," IEEE Trans. Antennas Propag., vol. 66, no. 8, pp. 3894-3901, Aug. 2018.

[18] H. L. Thal, "Radiation Efficiency Limits for Elementary Antenna Shapes," IEEE Trans. Antennas Propag., vol. 66, no. 5, pp. 2179-2187, May 2018.

[19] Md. S. I. Sagar et al., "Application of Machine Learning in Electromagnetics: Mini-Review," Electronics, vol. 10, no. 22, p. 2752, Nov. 2021.

[20] M.Li, R. Guo, K. Zhang, Z. Lin, F. Yang, S. Xu, X. Chen, A. Massa, A. Abubakar, "Machine Learning in Electromagnetics With Applications to Biomedical Imaging: A Review," IEEE Antennas Propag. Mag., vol. 63, no. 3, pp. 39-51, June 2021.

[21] F. Zardi, P. Nayeri, P. Rocca, R. Haupt, "Artificial Intelligence for Adaptive and Reconfigurable Antenna Arrays: A Review," IEEE Antennas Propag. Mag., vol. 63, no. 3, pp. 28-38, June 2021.

[22] A. Al-Jumaily, A. Sali, M. Riyadh, S. Q. Wali, L. Li, et A. F. Osman, "Machine Learning Modeling for Radiofrequency Electromagnetic Fields (RF-EMF) Signals from mmWave 5G Signals," IEEE Access, 2023.

[23] M. R. Khan, C. L. Zekios, S. Bhardwaj and S. V. Georgakopoulos, "A Deep Learning Convolutional Neural Network for Antenna Near-Field Prediction and Surrogate Modeling," in IEEE Access, vol. 12, pp. 39737-39747, 2024, doi: 10.1109/ACCESS.2024.3377219.

[24] H. El Misilmani, T. Naous, S. Al Khatib. 2020. "A Review on the Design and Optimization of Antennas Using Machine Learning Algorithms and Techniques," International Journal RF Microwave Computer-Aided Eng., Oct. 2020.

[25] N. Sarker et al., "Applications of Machine Learning and DeepLearning in Antenna Design, Optimization, and Selection: A Review," in IEEE Access, vol. 11, pp. 103890-103915, 2023.

[26] C. Gianfagna, M. Swaminathan, P. M. Raj, R. Tummala and G. Antonini, "Enabling antenna design with nano-magnetic materials using machine learning," 2015 IEEE Nanotechnology Materials and Devices Conference (NMDC), Anchorage, AK, USA, 2015, pp. 1-5, doi: 10.1109/NMDC.2015.7439256.

[27] P. Mahouti, "Design optimization of a pattern reconfigurable microstrip antenna using differential evolution and 3D EM simulation-based neural network model," Int J RF Microw Comput Aided Eng, vol. 29, no. 8, Apr. 2019.

[28] P. Mahouti, A. Kızılay, O. Tari, A. Belen and M. A. Belen, "Design Optimization of Ultra Wide Band Vivaldi Antenna Using Artificial Intelligence," 2021 International Applied Computational Electromagnetics Society Symposium (ACES), Hamilton, ON, Canada, 2021, pp. 1-4.

[29] H. Ahmed, Z. Xiaoping, H. Bello, and N. Iqbal, "Inverse design of multiparameter antenna using hybrid machine learning-driven training dataset," Microw. Opt. Technol. Lett., vol. 66, no. 1, 2023. https://doi.org/10.1002/mop.33691.

[30] M. S. Yahya, S. Soeung, S. K. A. Rahim, U. Musa, S. S. Ba Hashwan and M. A. Haque, "Machine Learning-Optimized Compact Frequency Reconfigurable Antenna With RSSI Enhancement for Long-Range Applications," in IEEE Access, vol. 12, pp. 10970-10987, 2024, doi: 10.1109/ACCESS.2024.3355145.

[31] Q. Wu, W. Chen, C. Yu, H. Wang and W. Hong, "Machine-Learning-Assisted Optimization for Antenna Geometry Design," in IEEE Trans. Antennas Propag., vol. 72, no. 3, pp. 2083-2095, March 2024, doi: 10.1109/TAP.2023.3346493

[32] J. Roqui, L. Santamaria, L. Khacef, A. Pegatoquet and L. Lizzi, "Estimation of Small Antenna Performance Using a Machine Learning Approach," in IEEE Int. Symp. Antennas Propag. and North American Radio Science Meeting, Montreal, Canada, 2020, pp. 581-582.

[33] B. S. Collins, "Practical application of small antennas in hardware platforms," in IET Microw. Antennas Propag., vol. 13, pp. 1883-1888, 2019, doi: 10.1049/iet-map.2018.5814.

[34] T. Houret, L. Lizzi, F. Ferrero, C. Danchesi and S. Boudaud, "DTC-Enabled Frequency-Tunable Inverted-F Antenna for IoT Applications," IEEE Antennas Wireless Propag. Lett., vol. 19, no. 2, pp. 307-311, Feb. 2020.

[35] L. Lizzi, F. Ferrero, C. Danchesi and S. Boudaud, "Design of antennas enabling miniature and energy efficient wireless IoT devices for smart cities," in IEEE International Smart Cities Conference, Trento, Italy, 2016, pp. 1-5.

[36] S. J. Pan and Q. Yang, "A Survey on Transfer Learning," IEEE Trans. Knowl. Data Eng., vol. 22, no. 10, pp. 1345-1359, Oct. 2010.

[37] N. Calik, F. Güneş, S. Koziel, A. Pietrenko-Dabrowska, M. A. Belen, and P. Mahouti, "Deep-learning-based precise characterization of microwave transistors using fully-automated regression surrogates," Scientific Reports, vol. 13, no. 1 (2023).

[38] D. Kingma and J. Ba, "Adam: A Method for Stochastic Optimization," International Conf. Learning Representations, Dec. 2014.

[39] C.-M. Kuan and K. Hornik, "Convergence of learning algorithms with constant learning rates," IEEE Transactions on Neural Networks, vol. 2, no. 5, pp. 484-489, Sept. 1991.

[40] T. Szandala, "Review and comparison of commonly used activation functions for deep neural networks," Bio-inspired Neurocomputing, p. 203-224, 2021.
[41] C. Nwankpa, W. Ijomah, A. Gachagan, and S. Marshall, "Activation Functions: Comparison of Trends in Practice and Research for Deep Learning," http://arxiv.org/abs/1811.03378., 2018.
[42] Q. Wang, Y. Ma, K. Zhao, *et al.*, "A Comprehensive Survey of Loss Functions in Machine Learning," Ann. Data. Sci. 9, 187–212 (2022). https://doi.org/10.1007/s40745-020-00253-5
[43] A. Gholamy, V. Kreinovich, O. Kosheleva, "Why 70/30 or 80/20 Relation between Training and Testing Sets: A Pedagogical Explanation," Dep. Tech. Rep. (CS) 2018, 11, 105–111. Available online: https://scholarworks.utep.edu/cs_techrep/1209
[44] J. D. Rodriguez, A. Perez and J. A. Lozano, "Sensitivity Analysis of k-Fold Cross Validation in Prediction Error Estimation," in IEEE Trans. Pattern Analysis Machine Intell., vol. 32, no. 3, pp. 569-575, Mar. 2010.
[45] L. Khacef, N. Abderrahmane and B. Miramond, "Confronting machine-learning with neuroscience for neuromorphic architectures design," in International Joint Conference on Neural Networks, Rio de Janeiro, Brazil, 2018, pp. 1-8.
[46] V. Sze, Y. Chen, T. Yang and J. S. Emer, "Efficient Processing of Deep Neural Networks: A Tutorial and Survey," Proc. IEEE, vol. 105, no. 12, pp. 2295-2329, Dec. 2017.
[47] M. Abadi et al., "TensorFlow: Large-Scale Machine Learning on Heterogeneous Systems," http://download.tensorflow.org/paper/whitepaper2015.pdf, 2015.
[48] B. L. G. Jonsson, F. Ferrero, S. Shi and L. Wang, "Optimal Bandwidth Positions for a Terminal Embedded Antenna: Physical Bounds and Antenna Design," IEEE Trans. Antennas Propag., vol. 69, no. 4, pp. 1931-1941, April 2021.

Julian ROQUI(Student Member, IEEE) received the M.Sc. degree in electronic telecommunication engineering from the Faculté des Sciences, Université Côte d'Azur, Nice, France, in 2021. He is currently pursuing the Ph.D. degree with the Laboratory of Electronics, Antennas, and Telecommunications, Université Côte d'Azur. At the moment, his research focuses on the development of Machine Learning algorithms in order to predict the maximum achievable performance of miniature antenna systems for future Internet-of-Things networks and 5G applications.

Alain PEGATOQUET(Member, IEEE) received the M.Sc. and Ph.D. degrees in electrical and computer engineering from the University of Nice Sophia Antipolis (UNS), Nice, France, in 1995 and 1999, respectively. After nine years of experience in the industry as a System DSP Engineer in VLSI technology at Texas Instruments, Dallas, TX, USA, he joined the University Côte d'Azur (UCA), Nice, as an Associate Professor in 2008. He is currently leading the Edge computing and DiGital systEms (EDGE) Team, Laboratory of Electronics, Antennas and Telecommunications (LEAT), a mixed research unit from UCA and CNRS, Paris, France. He has authored or coauthored more than 125 scientific publications and holds two patents. He has collaborated with several universities and research centers, such as ETH Zürich, Zürich, Switzerland; the University of Verona, Verona, Italy; the University of Rennes—IRISA, Rennes, France. His research interests include embedded AI, edge computing, IOT and low-power management policies. Pr. Pegatoquet was the General Co-Chair of the IEEE Sensors Applications Symposium (SAS) 2019, Sophia Antipolis, France.

Luca SANTAMARIA(Student Member, IEEE) received the first M.Sc. degree in computer science from the Faculté des Sciences, Université Côte d'Azur, Nice, France, and the second M.Sc. degree in telecommunications engineering from the Politecnico di Bari, Bari, Italy, in 2018. He is currently pursuing the Ph.D. degree with the Laboratory of Electronics, Antennas, and Telecommunications, Université Côte d'Azur. At the moment, his research focuses on the development of miniature and low-power reconfigurable antenna systems for future Internet-of-Things networks.

Leonardo LIZZI(Senior Member, IEEE) is currently an Associate Professor at the University Côte d'Azur (UCA), France. He received the master's degree in Telecommunication Engineering and the Ph.D. degree in Information and Communication Technology from the University of Trento, Italy, in 2007 and 2011, respectively. During his Ph.D. he has been visiting researcher at the Pennsylvania State University, USA, and the University of Nagasaki, Japan. From 2011 to 2014 he was Post-Doctoral researcher at the Laboratory of Electronics, Antennas, and Telecommunications (LEAT) of UCA. At the moment, his research focuses on reconfigurable, miniature, multi-standards antennas for Internet-of-Things applications, wearable devices, and 5G terminals. He is the coordinator of the European School of Antennas (ESoA) Ph.D. course on "Antennas and Rectennas for IoT Applications (ARIA)". He is co-author of more than 140 papers in international journals and conference proceedings.